Lattice-gas automata with attractive and repulsive interactions

M. Gerits and M. H. Ernst
Institute for Theoretical Physics, Princetonplein 5, P.O. Box 80006, 3508 TA Utrecht, The Netherlands

D. Frenkel
FOM–Institute for Atomic and Molecular Physics, Kruislaan 407, 1098 AJ Amsterdam, The Netherlands
(Received 20 November 1992)

Particles interacting as square wells or square barriers of finite range r are modeled as a two-dimensional lattice gas, in the spirit of the liquid-gas model of Appert and Zalesky [Phys. Rev. Lett. **64**, 1 (1990)]. If r is sufficiently large, the system exhibits phase separation. We derive the equation of state, which is of the van der Waals type. If it has an unstable branch, the Maxwell construction is used. Analytical expressions for the transport coefficients as functions of r are calculated from the decay rates of the hydrodynamic modes. The theoretical results for thermodynamic and transport properties show good agreement with extensive computer simulations.

PACS number(s): 05.20.Dd, 47.20.Hw, 64.60.Ht, 51.10.+y

I. INTRODUCTION

The lattice-gas automata (LGA's) most frequently considered deal only with point particles [1]. By adding a long-range attraction to the triangular lattice gas, several authors [2–4] have constructed "liquid-gas" models that can undergo phase separation, when the range r of the attractive force is sufficiently large. The force is impulsive, and only different from zero when the distance equals the range r. Both properties are characteristic for particles interacting with a square-well attraction or square-barrier repulsion. All interactions conserve number and momentum, and observe the Fermi exclusion rule.

In trying to understand and calculate the equilibrium and transport properties of LGA's several fundamental problems are encountered, such as the validity of the laws of thermodynamics, and the existence of the Gibbs state. The first one concerns the derivation and interpretation of the first and second laws of thermodynamics [5–7] and the meaning of temperature and pressure. In the present paper we further restrict ourselves to systems with vanishing total momentum (systems macroscopically at rest). Furthermore, problems related to the non-Galilean factor $g(\rho)$ are not addressed here, because they are related to nonlinear terms in the equations of fluid dynamics [1]. The analysis in this paper is based on hydrodynamic modes, which only involve the linearized Navier-Stokes equations. In LGA's the kinetic pressure or momentum flux density p, which is the pressure based on the virial theorem, does not coincide with the "thermodynamic pressure," which is obtained as the derivative of the logarithm of the partition function with respect to the volume. This difference occurs also in the standard LGA's with purely local collision rules, as already noted in Ref. [5]. For instance, in the Frisch, Hasslacher, and Pomeau (FHP) [1] models the kinetic pressure is $p=3f$, and the "thermodynamic pressure," is $p_{\rm th}=-3\ln(1-f)$, where $f=\frac{1}{7}\rho$ is the reduced density. Very recently Cercignani has been able to derive the laws of thermodynamics from a discrete velocity Boltzmann equation with continuous space and time variables [7]. His Boltzmann equation supports the conservation laws of number, momentum, and energy, and no Fermi exclusion is imposed. His derivation supports the temperature definition for LGA's used in Refs. [6,8]. It shows that the kinetic pressure differs from $\rho k_B T$, even if the particles obey Boltzmann statistics. He also clarifies the thermodynamic meaning of $p_{\rm th}$—it is not a pressure—and he shows that the difference between p and $p_{\rm th}$ is related to the lack of Galilean invariance, or equivalently to the limited number of velocity states. It is to be expected that his arguments can be extended to the statistical mechanics of lattice-gas cellular automata, but this has still to be done.

The second fundamental problem concerns the existence or nonexistence of a Gibbs state and the validity of statistical mechanics for LGA's. There are detailed and nondetailed balance models. The first class obeys the detailed balance conditions, or the weaker Stueckelberg [9] or semidetailed balance conditions [1,10]. For these models the Gibbs state is the equilibrium state. The partition function and thermodynamic potential can be calculated. For models that violate the above conditions the equilibrium state is not the Gibbs state. It is unknown [11–13], and the partition function cannot be calculated. The nonlocal interactions of the present model violate the conditions of detailed or semidetailed balance. All analytic results for such nondetailed balance models are based on mean-field theory or the Boltzmann equation, in which all existing correlations [11,13,14] are neglected by making a molecular chaos assumption. The same assumptions will be made here when calculating the equation of state and transport properties of our LGA with finite-range attraction or repulsion.

Our main goal here is to develop quantitative theoretical predictions for the thermodynamic and transport properties of such models, and to test the theories against results from computer simulations. In Sec. II the dynamics of the attractive model is defined. The microscopic

1063-651X/93/48(2)/988(12)/$06.00

and macroscopic properties of the model with attraction are related to those with repulsion through a duality transformation. In Sec. III the nonlinear Boltzmann equation is constructed, which involves three steps: (i) finite-range collisions, (ii) local collisions, and (iii) propagation, and the equation of state is derived. It has a van der Waals type loop for long-range attractive forces, which indicates that the system can undergo a phase separation [2]. In Sec. IV we calculate the eigenvalues corresponding to the slow hydrodynamic modes of the linearized Boltzmann equation, and extract from them in Sec. V the transport coefficients as a function of the interaction range. In Sec. VI we will show that the pressure in the metastable fluid phase, as well as in the region of coexisting phases, obtained from the Maxwell construction, is in good agreement with the simulation results [2,11], and the same holds for the speed of sound. The analytical calculations and computer simulations of the transport coefficients are compared in Sec. V II, and we conclude with a discussion in Sec. V III. After completion of this paper a theoretical computation of transport coefficients for a similar model has also been given by Appert, Zaleski, and d'Humières [15].

II. FINITE-RANGE INTERACTIONS

A. Microdynamic equation

The model is based on the triangular lattice gas, referred to as the FHP III model [16] with a maximum of six moving and one resting particle per node. The model describes a gas of point particles, obeying the Fermi exclusion rule, and evolving in time under strictly local collision rules. The particles are described in terms of occupation numbers $n_i(x,t)$, where the two-dimensional vector $\mathbf{x}$ denotes a node of the triangular lattice, and where i ($i=1,2,\ldots,6$) labels an allowed velocity or nearest-neighbor (NN) lattice vector $\mathbf{c}_i$. The label $i=0$ refers to the rest particle with $\mathbf{c}_0=\mathbf{0}$. (Regarding notation: whenever $\mathbf{x}$, $\mathbf{c}_i$, $\mathbf{k}$ with magnitude $|x|$, $|c_i|$, $|k|$ appear as arguments of a function, they are simply written as x, c_i, k.)

The nonlocal attraction is modeled as an impulsive force of range r, comparable with a square-well potential. It acts only along any of the six NN lattice vectors $\mathbf{c}_i$, and only when two particles, separated by r lattice units, are in an interacting configuration. All interacting configurations of the present model are shown in Fig. 1. The solid arrow denotes a particle, described by $n_i(x,t)$, and the open arrow a hole, described by $\bar{n}_i(x,t)=1-n_i(x,t)$. The interactions occur irrespective of the occupation of links, not labeled with arrows. All interactions conserve total momentum. In the collisions (a), (b), and (c) an amount of momentum $\mathbf{c}_j$,$\mathbf{c}_j$, and $2\mathbf{c}_j$, respectively, is instantaneously exchanged over a distance r, in the direction $-\mathbf{c}_j$, between particles of the interacting pair. In repulsive interactions the instantaneous transfer of momentum is in the opposite direction. The mechanism of instantaneous transfer of momentum from one particle to another one at a different position, is called collisional transfer [17]. It is the dominant transport mechanics in dense liquids.

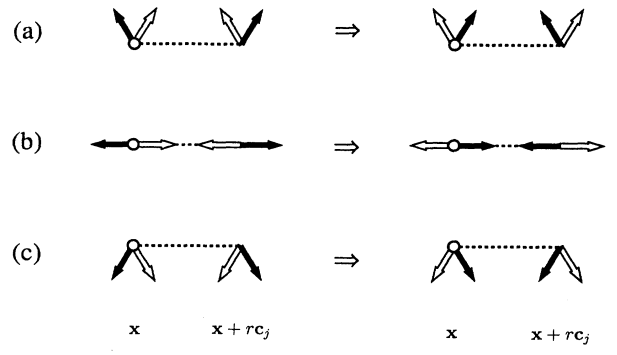

FIG. 1. Nonlocal collision rules for attractive interactions in direction $\mathbf{c}_j$. Solid (open) arrows represent particles (holes).

Next we formalize the description. The dynamics of the present LGA consists of the three steps: (i) a finite-range attraction step; its action on the occupation number is denoted by

$$n_i'(x,t)=\mathcal{L}_i(n(t)) \; ; \tag{2.1}$$

(ii) a local collision step, denoted by

$$n_i''(x,t)=\mathcal{I}_i(n'(t)) = n_i'(x,t)+I_i(n'(t)) \; , \tag{2.2}$$

where $I_i(n)$ in the present paper is the standard nonlinear collision term of the FHP III model [16], (iii) a propagation step, denoted by

$$n_i(x+c_i,t+1)=n_i''(x,t) \; . \tag{2.3}$$

Combination of the three steps yields the microdynamic equation, formally written as

$$n_i(x+c_i,t+1)=\mathcal{I}_i(\mathcal{L}(n(t))) \; . \tag{2.4}$$

Steps (ii) and (iii) are standard [1], with the following additional specification. In the cases of binary and quadrupole collisions with two possible outcomes (rotations of the ingoing configuration over $+2\pi/3$ or $-2\pi/3$) we choose at every collision step either the (+)- or the (−)-rotation for all nodes in the lattice simultaneously, with a probability of $\frac{1}{2}$. A cyclic permutation of the three steps generates the same dynamics. Permutation of steps (i) and (ii) defines a somewhat different dynamics. The chosen order defines the model. In the next section we concentrate on the attractive interaction.

B. Attraction

The three possible attractive interactions in Fig. 1 are independent of each other and may occur simultaneously. Furthermore there are three possible directions along which this force is acting. At a given time step t one direction is chosen at random and applies to all attractive interactions on the entire lattice.

To make the formal description more explicit we consider an attractive interaction, parallel to $\mathbf{c}_j$, with a collision term, denoted by $L_i^j(n)$ with $j=i$, $i+1$, $i-1$. It modifies the occupation number $n_i(x,t)$ of velocity chan-

nel $\mathbf{c}_i$ as

$$n_i'(x,t)=n_i(x,t)+L_i^j(n(t)) \ . \tag{2.5}$$

The complete collision operator is then given by $\alpha L_i^{i+1}+\beta L_i^i+\gamma L_i^{i-1}$, where α, β, and γ are Boolean variables, satisfying $\alpha+\beta+\gamma=1$ with expectation values $\langle\alpha\rangle=\langle\beta\rangle=\langle\gamma\rangle=\frac{1}{3}$. The average $\langle\ \rangle$ is taken over the ensemble of realizations of the Boolean variables α,β,γ, which are drawn at every time step. Combining the different j directions and taking the average $\langle\ \rangle$ yields then

$$\begin{aligned}\langle n_i'\rangle&=\langle n_i\rangle+\tfrac{1}{3}[\langle L_i^i(n)\rangle+\langle L_i^{i+1}(n)\rangle+\langle L_i^{i-1}(n)\rangle]\\&\equiv\mathcal{L}_i(n) \ .\end{aligned} \tag{2.6}$$

The collision terms L_i^j consist of a gain term and a loss term, which can be constructed from Fig. 1 with the result

$$\begin{aligned}L_i^i(n)&=[\bar{n}_i n_{i+3}](x)[n_i\bar{n}_{i+3}](x+rc_i)\\&\quad-[n_i\bar{n}_{i+3}](x)[\bar{n}_i n_{i+3}](x-rc_i) \ ,\\L_i^{i\pm1}(n)&=[\bar{n}_i n_{i\mp1}](x)[n_i\bar{n}_{i\mp1}](x+rc_{i\pm1})\\&\quad-[n_i\bar{n}_{i\mp1}](x)[\bar{n}_i n_{i\mp1}](x-rc_{i\pm1}) \ ,\end{aligned} \tag{2.7}$$

where we have introduced the shorthand notation, $[\bar{n}_j n_l](y)=\bar{n}_j(y)n_l(y)$.

C. Repulsion: Dual model

To model repulsive interactions in LGA's the square well of the previous section can be replaced by a barrier of width r. The interacting configurations with corresponding transitions are also defined through Fig. 1 if open arrows represent particles and solid ones empty states or holes. Again, the occupation of the remaining links is irrelevant for the occurrence of the transitions. The repulsive interaction also conserves total momentum. The collisions (a), (b), and (c) of Fig. 1 transfer the same amount of momentum as in the attractive case, but now in the opposite direction. Consequently, by interchanging particles and holes, i.e., by interchanging n_i and $\bar{n}_i$ in (2.6) and (2.7), the attractive interactions become repulsive and vice versa. Because the local collision rules of the FHP III model are self-dual, the LGA with repulsive interaction is the dual model of the one with attractive interactions.

If we denote the properties of the repulsive and attractive model, respectively, with and without an overline, the duality transformation, $f\leftrightarrow1-f$, gives the following relations:

$$\begin{aligned}&\bar{p}(\rho)=3-p(7-\rho), \quad \bar{c}_s(\rho)=c_s(7-\rho) \ ,\\&\bar{\nu}(\rho)=\nu(7-\rho), \quad \bar{\gamma}(\rho)=\gamma(7-\rho) \ .\end{aligned} \tag{2.8}$$

Here $p(\rho)$ is the pressure, $c_s(\rho)$ the speed of sound, $\nu(\rho)$ the kinematic viscosity, and $\gamma(\rho)$ the sound damping constant in a system that is macroscopically at rest. As an illustration of this duality relation we show in Fig. 2 the pressure as a function of density for the attractive model [Fig. 2(a)] and for its dual, the repulsive model [Fig. 2(b)].

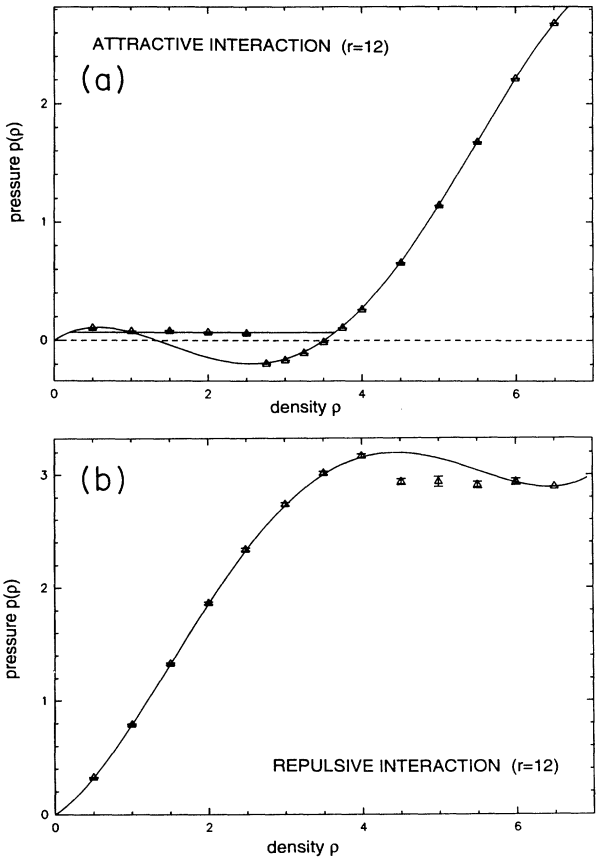

FIG. 2. Equation of state $p(\rho)$ with Maxwell construction. Interaction range $r=12$ (a) with attractive interactions and (b) [dual model of (a)] with repulsive interactions. In stable and metastable regions the simulations agree with the van der Waals equation; in the unstable region simulations yield the coexistence pressure $p_0\simeq0.068$.

III. MEAN-FIELD THEORY

A. Nonlinear Boltzmann equation

As a first attempt to describe the thermodynamic and transport properties of this model, we construct a mean-field theory by neglecting at every time step the correlations between occupation numbers in different velocity directions and on different nodes. The distribution function $f_i(x,t)=\langle n_i(c,t)\rangle_{\rm ne}$ is the average occupation number, averaged over some nonequilibrium initial ensemble. It also includes the average defined below (2.5). The mean-field approximation is implemented by averaging the microdynamic equation (2.4) over this nonequilibrium state and by subsequently making the molecular chaos assumption. The result is the nonlinear Boltzmann equation for the present model.

$$\begin{aligned}f_i(x+c_i,t+1)&=\langle\mathcal{I}_i(\mathcal{L}(n(t)))\rangle_{\rm ne}\\&=\mathcal{I}_i(\mathcal{L}(\langle n(t)\rangle_{\rm ne}))=\mathcal{I}_i(\mathcal{L}(f(t))) \ ,\end{aligned} \tag{3.1}$$

where the local collision operator $\mathcal{I}(f)$ is given by (2.2)

and the nonlocal one $\mathcal{L}(f)$ by (2.6) and (2.7).

If the total moment of the system is vanishing, the Boltzmann equation admits the uniform distribution $f_i(x,\infty)=f$ with $i=0,1,2,\ldots,6$, as a stationary distribution. This can be verified from (2.2) and (2.4)–(2.7). The uniform equilibrium state is, however, not necessarily stable. As we shall see in the next section, the system undergoes a phase separation into a light and a heavy phase, if the range of the attractive interaction is sufficiently large.

B. Equation of state

The local and nonlocal interactions conserve momentum. Consider the local momentum density

$$\mathbf{g}(x,t)=\rho(x,t)\mathbf{u}(x,t)=\sum_i \mathbf{c}_i f_i(x,t) , \tag{3.2}$$

where $\rho(x,t)$ and $\mathbf{u}(x,t)$ are the local density and local flow velocity. For large spatial and temporal scales, the local conservation law can be written as $\partial_t \rho\mathbf{u}=-\nabla\cdot\mathsf{P}$, where P is the local pressure tensor. As we are only interested in obtaining the local equilibrium pressure, it suffices for our purpose to derive the linearized Euler equation, where quadratic and higher-order deviations from equilibrium and higher-order gradients have been neglected.

In deriving the explicit form of $\mathsf{P}(x,t)$ we first observe that the FHP III collision rules in (2.2) satisfy $\sum_i \mathbf{c}_i I_i(f)=\mathbf{0}$. Multiplication of (2.4) with $\mathbf{c}_i$ and summation over i yields, with the help of (2.1)–(2.7),

$$\begin{aligned}\sum_i \mathbf{c}_i f_i(x+c_i,t+1)&=\sum \mathbf{c}_i f_i'(x,t)=\sum_i \mathbf{c}_i \mathcal{L}_i(f(t))\\ &=\sum_i \mathbf{c}_i f_i(x,t)+\tfrac{1}{3}\sum_{j,i}\mathbf{c}_i L_i^j(f(t)) ,\end{aligned} \tag{3.3}$$

where $n=i,i\pm1$. Inspection of (2.7) shows that the nonlocal collision term L_i^n can be approximated, in a long-wavelength limit, by

$$L_i^n(f)=(T_n-1)\mathcal{E}_i^n(f)\simeq\nabla\cdot r\mathbf{c}_n\mathcal{E}_i^n(f) , \tag{3.4}$$

where $T_n g(x)=g(x+rc_n)$. Taylor expansion of the left-hand side of (3.3) and use of (3.4) yields the pressure tensor correct to $O(\nabla)$ excluded, i.e.,

$$\mathsf{P}(x,t)=\sum_i \mathbf{c}_i\mathbf{c}_i f_i(x,t)-\tfrac{1}{3}r\sum_{n,i}\mathbf{c}_n\mathbf{c}_i\mathcal{E}_i^n(f) , \tag{3.5}$$

where $n=i,i\pm1$ and

$$\begin{aligned}\mathcal{E}_i^i(f)&=[f_i\bar{f}_{i+3}](x)[\bar{f}_i f_{i+3}](x-rc_i) ,\\ \mathcal{E}_i^{i\pm1}(f)&=[f_i\bar{f}_{i\mp1}](x)[\bar{f}_i f_{i\mp1}](x-rc_{i\pm1}) ,\end{aligned} \tag{3.6}$$

with $\bar{f}_i=1-f_i$. The first term in (3.5) represents the kinetic transport, the second the collisional transfer. In global equilibrium, where $f_i(x,\infty)=f=\rho/7$, the pressure tensor, $\mathsf{P}_{\alpha\beta}(x,\infty)=p\delta_{\alpha\beta}$, is diagonal and the pressure follows from (3.5) and (3.6),

$$\begin{aligned}p&=3f-2rf^2(1-f)^2\\ &=c_0^2[\rho-\tfrac{2}{21}r\rho^2(1-\rho/7)^2] .\end{aligned} \tag{3.7}$$

Here $c_0=\sqrt{3/7}$ is the speed of sound in the FHP III model. The speed of sound c_s in the present model with long-range attraction is

$$c_s^2=\frac{dp}{d\rho}=c_0^2(1-\tfrac{4}{3}rf(1-f)(1-2f))\equiv c_0^2(1-\tfrac{4}{3}r\kappa_3) , \tag{3.8}$$

provided $dp/d\rho$ is positive. This is not the case in the spinodal region, where $dp/d\rho<0$. Pressure and speed of sound for the repulsive LGA follow from the duality transformation $f\leftrightarrow 1-f$, which implies in (3.7) and (3.8) the replacement $r\rightarrow -r$.

A similar expression for the pressure has been derived in Refs. [2,4] for models with long-range attraction. For $r\neq 0$ the pressure $p(\rho)$ has two inflection points, at $\rho=\rho_-\sim 1.48$ and at $\rho=\rho_+\sim 5.52$, independent of r. If the range r is sufficiently large, the pressure curve has a loop if $(dp/d\rho)_{\rho_-}=3-4r\kappa_3(\rho_-)\leq 0$. This is the case for $r\geq 8$. At the second inflection point ρ_+ the slope $(dp/d\rho)_{\rho_+}$ is positive.

The equation of state for $r\geq 8$ has metastable and unstable branches. We have indeed observed that the system undergoes a phase separation into a light gas phase and a heavy fluid phase of reduced densities ρ_g and ρ_l, respectively, as is known in the literature [2–4]. In the region of coexisting phases, $\rho_g<\rho<\rho_l$, the pressure remains equal to a constant p_0 and the values of p_0, ρ_g, and ρ_l are obtained from the Maxwell construction, as shown in Fig. 2(a) for $r=12$. Here one finds for the pressure in the coexisting phase $p_0=0.068$, for the gas density $\rho_g=0.20$, and for the liquid density $\rho_l=3.65$.

IV. LINEARIZED BOLTZMANN EQUATION

A. Eigenvalue equation

In this section deviations, $\delta f_i(x,t)=f_i(x,t)-f$, from the uniform equilibrium state will be analyzed in terms of eigenmodes, i.e., we look for solutions of the Boltzmann equation (3.1) of the form

$$\delta f_i(x,t)=\psi_\mu(k,c_i)\exp[ik\cdot x+z_\mu(k)t] , \tag{4.1}$$

where $z_\mu(k)$ represents the eigenvalue of the mode ψ_μ. Here we are only interested in the hydrodynamic or slow modes, which correspond to the conservation laws, and satisfy $z_\mu(k)\rightarrow 0$ as $k\rightarrow 0$. If $\mathrm{Im}z_\mu(k)=c_s(k)|k|$ is nonvanishing, we are dealing with a sound mode with a propagation speed $c_s(k)$. The real part $\mathrm{Re}z_\mu(k)<0$ represents the damping.

The two-dimensional system under consideration conserves total particle number and momentum. There exist three corresponding hydrodynamic modes: one shear mode or transverse velocity mode, $\psi_v(k,c)$, and two sound modes $\psi_\sigma(k,c)$ $(\sigma=\pm)$. In the long-wavelength

limit the eigenvalues have the following form:

$$z_\nu(k)=-\nu|k|^2 ,$$
$$z_\sigma(k)=-i\sigma c_s|k|-\gamma|k|^2 , \tag{4.2}$$

where ν is the kinematic viscosity and γ the sound damping constant. This method provides an alternative to the Chapman-Enskog method for determining the linear transport coefficients ν and γ [18]. The method has been extended recently to LGA's [8].

The composite collision operator $\mathcal{I}(\mathcal{L}(f(t)))$ involves two nonlinear operators $\mathcal{I}$ and $\mathcal{L}$. Linearization of the local collision operator $\mathcal{I}$ in (2.2) gives the Boltzmann collision operator of the standard FHP III model [19],

$$\delta f_i''(x,t)=\delta f_i'(x,t)+I_i(f+\delta f'(t))$$
$$=(1+\Omega)_{ij}\delta f_j'(x,t) , \tag{4.3}$$

where $I_i(f)=0$ for the uniform distribution. Terms quadratic in δf_i have been neglected, Ω_{ij} with $(i,j=0,1,2,\ldots,6)$ is a 7×7 matrix. Einstein convention has been used for repeated indices.

The nonlocal attractive interaction term (2.6) and (2.7) gives after linearization for plane-wave excitations (4.1),

$$\delta f_i'(x,t)=\delta f_i(x,t)+\tfrac{1}{3}\sum_{n=i,i\pm1} L_i^n(f+\delta f(t))$$
$$=(1+\Lambda(k))_{ij}\delta f_j(x,t) , \tag{4.4}$$

where $L_i^n(f)=0$ for the uniform distribution. Note that $\Lambda(k)$ depends on the wave number k because the attraction operator is nonlocal. Combination of the linearized collision operators (2.1) [step (i)] and (2.2) [step (ii)] with the propagation step (iii) in (2.3) yields the linearized version of (2.4) or (3.1), i.e.,

$$[\mathcal{S}(k)(1+\Omega)(1+\Lambda(k))]_{ij}\psi_\mu(k,c_j)=e^{z_\mu(k)}\psi_\mu(k,c_i) , \tag{4.5}$$

where $\mathcal{S}_{ij}(k)=e^{-\iota k\cdot c_i}\delta_{ij}$ is the (diagonal) propagation matrix. This linear set of equations for the eigenmodes $\psi_\mu(k,c_j)$ $(j=0,1,2,\ldots,6)$ and eigenvalues $z_\mu(k)$ with $z_\mu(k)\to0$ for $k\to0$, will be solved in Sec. V for the hydrodynamic modes by perturbation theory.

B. Finite-range collision operator

In this section the explicit form of the nonlocal interaction operator $\Lambda_{ij}(k)$ is constructed, and some useful properties are derived. Starting from (2.6) and (2.7) we obtain

$$\Lambda_{ij}(k)a_j\equiv\tfrac{1}{3}\sum_{n=i,i\pm1} L_i^n(f+a)+O(a^2)$$
$$=\tfrac{1}{3}\iota\kappa_3\{(a_i+a_{i+3})\sin rk\cdot c_i+(a_i+a_{i-1})\sin rk\cdot c_{i+1}+(a_i+a_{i+1})\sin rk\cdot c_{i-1}\}$$
$$-\tfrac{1}{3}\kappa_2\{(a_i-a_{i+3})(1-\cos rk\cdot c_i)+(a_i-a_{i-1})(1-\cos rk\cdot c_{i+1})+(a_i-a_{i+1})(1-\cos rk\cdot c_{i-1})\} , \tag{4.6}$$

where $\iota=\sqrt{-1}$. For the determination of the transport coefficients ν and γ in (4.2) only the long-wavelength behavior of $\Lambda(k)$ is required. We therefore expand (4.6) in powers of k. Collecting results to $O(k^2)$ yields

$$\Lambda_{ij}(k)a_j\equiv(\Lambda(k)|a\rangle)_i$$
$$=(\iota k)\Lambda_{ij}^{(1)}a_j+(\iota k)^2\Lambda_{ij}^{(2)}a_j+\cdots . \tag{4.7}$$

The matrices $\Lambda^{(1)}$ and $\Lambda^{(2)}$ are defined as

$$(\Lambda^{(1)}|a\rangle)_i=\tfrac{1}{3}r\kappa_3\{c_{li}(a_i+a_{i+3})+c_{l,i+1}(a_i+a_{i-1})+c_{l,i-1}(a_i+a_{i+1})\} ,$$
$$(\Lambda^{(2)}|a\rangle)_i=\tfrac{1}{6}r^2\kappa_2\{c_{li}^2(a_i-a_{i+3})+c_{l,i+1}^2(a_i-a_{i-1})+c_{l,i-1}^2(a_i-a_{i+1})\} , \tag{4.8}$$

where $c_{li}\equiv\hat{\mathbf{k}}\cdot\mathbf{c}_i$ and $a_i\equiv a(c_i)$ are the components of a seven-vector $(i=0,1,2,\ldots,6)$ and $\hat{\mathbf{k}}$ a unit vector. We further introduced

$$\kappa_2=f(1-f) ,$$
$$\kappa_3=f(1-f)(1-2f) . \tag{4.9}$$

In the evaluation of the formulas, to be obtained in the next section, one needs $\Lambda|a\rangle$ for $a=\{1,c_l,c_\perp\}$ where $c_\perp=\hat{\mathbf{k}}_\perp\cdot\mathbf{c}$ is the transverse component of $\mathbf{c}$. It requires straightforward but lengthy algebra. The result is

$$\Lambda^{(1)}|1\rangle=\tfrac{4}{3}r\kappa_3|c_l\rangle,\quad \langle1|\Lambda^{(1)}=0 ,$$
$$\Lambda^{(1)}|c_l\rangle=\tfrac{1}{2}r\kappa_3|c_l^2-c_\perp^2\rangle ,$$
$$\langle c_l|\Lambda^{(1)}=\tfrac{2}{3}r\kappa_3\langle c^2|+\tfrac{1}{6}r\kappa_3\langle c_l^2-c_\perp^2| , \tag{4.10}$$
$$\Lambda^{(1)}|c_\perp\rangle=r\kappa_3|c_lc_\perp\rangle,\quad \langle c_\perp|\Lambda^{(1)}=\tfrac{1}{3}r\kappa_3\langle c_lc_\perp| .$$

Here we introduced the symbol $(\langle a|\Lambda)_i=a_j\Lambda_{ji}$. The two nonvanishing matrix elements of $\Lambda^{(2)}$ in the subspace, spanned by $|1\rangle$, $|c_l\rangle$, and $|c_\perp\rangle$, are

$$\langle c_l|\Lambda^{(2)}|c_l\rangle=\tfrac{9}{8}r^2\kappa_2 ,$$
$$\langle c_\perp|\Lambda^{(2)}|c_\perp\rangle=\tfrac{3}{8}r^2\kappa_2 , \tag{4.11}$$

where also the scalar product $\langle a|b\rangle=\sum_i a_i b_i$ has been introduced.

V. PROPAGATION AND DAMPING CONSTANTS

A. Perturbation theory

To solve the eigenvalue problem (4.5) for the hydrodynamic modes it is convenient to write (5.1) in the form

$$\{e^{z_\mu(k)+\iota k\cdot c}-(1+\Omega)[1+\Lambda(k)]\}_{ij}\psi_\mu(k,c_j)=0 \tag{5.1}$$

and expand the different terms in powers of the wave number,

$$\begin{aligned} z_\lambda(k)&=(\iota k)z_\lambda^{(1)}+(\iota k)^2 z_\lambda^{(2)}+\cdots ,\\ \psi_\lambda(k)&=\psi_\lambda^{(0)}+(\iota k)\psi_\lambda^{(1)}+(\iota k)^2\psi_\lambda^{(2)}+\cdots ,\\ \Lambda(k)&=(\iota k)\Lambda^{(1)}+(\iota k)^2\Lambda^{(2)}+\cdots , \end{aligned} \tag{5.2}$$

and inserting the expansions into the eigenvalue equation (5.1), to yield

$$\begin{aligned} &\Omega|\psi_\mu^{(0)}\rangle=0 ,\\ &\Omega|\psi_\mu^{(1)}\rangle=[c_l+z_\mu^{(1)}-(1+\Omega)\Lambda^{(1)}]|\psi_\mu^{(0)}\rangle ,\\ &\Omega|\psi_\mu^{(2)}\rangle=[\tfrac{1}{2}(c_l+z_\mu^{(1)})^2+z_\mu^{(2)}-(1+\Omega)\Lambda^{(2)}]|\psi_\mu^{(0)}\rangle\\ &\qquad\qquad+[c_l+z_\mu^{(1)}-(1+\Omega)\Lambda^{(1)}]|\psi_\mu^{(1)}\rangle . \end{aligned} \tag{5.3}$$

To obtain the transport coefficients in (4.2) one needs $z_\mu^{(2)}$, which can be obtained from the second-order equation in (5.3). Consider first the solution of the zeroth-order equation, which is an arbitrary linear combination of collisional invariants a_n, i.e.,

$$\begin{aligned} |\psi_\mu^{(0)}\rangle&=A_\rho|1\rangle+A_l|c_l\rangle+A_\perp|c_\perp\rangle\\ &\equiv\sum_n A_n|a_n\rangle . \end{aligned} \tag{5.4}$$

The eigenvalue problem to zeroth order is threefold degenerate. The collisional invariants $a_n=\{1,c_l,c_\perp\}$ are right and left zero eigenvectors of the symmetric matrix Ω.

The higher-order inhomogeneous equations in (5.3) are only soluble if the inhomogeneous term, say, R is orthogonal to the zero subspace, i.e., $\langle a_n|R\rangle=0$. This yields the first-order eigenvalue problem:

$$\sum_m\langle a_n|z_\mu^{(1)}+c_l-\Lambda^{(1)}|a_m\rangle A_m=0 , \tag{5.5}$$

where a_n with $(n=\rho,l,\perp)$ are the collisional invariants. The matrix $\Lambda^{(1)}$, defined in (4.8), *not symmetric.* Consequently, its right eigenvectors $|\psi_\mu^{(0)}\rangle$ are not orthogonal, but form a biorthogonal set together with the left eigenvectors $\langle\tilde\psi_\mu^{(0)}|$, i.e.,

$$\langle\tilde\psi_\mu^{(0)}|\psi_{\mu'}^{(0)}\rangle=\mathcal{N}_\mu\delta_{\mu\mu'} , \tag{5.6}$$

where $\mathcal{N}_\mu$ is a normalization constant. The matrix elements in (5.5) can be calculated with the help of the properties (4.10). The only nonvanishing matrix elements of $M=c_l-\Lambda^{(1)}$ in the zero subspace a_n are

$$\begin{aligned} M_{\rho l}&=\langle c_l|c_l\rangle=7c_0^2=3 ,\\ M_{l\rho}&=\langle c_l|c_l-\Lambda^{(1)}|1\rangle\\ &=7c_0^2(1-\tfrac{4}{3}r\kappa_3)=7c_s^2 . \end{aligned} \tag{5.7}$$

In the region where $c_s^2=dp/d\rho$ is positive, c_s is the speed of sound in the nonlocal attractive LGA [see (3.8) and (4.9)], and c_0 the speed of sound of the standard FHP III model. In the spinodal region $c_s^2=dp/d\rho<0$. This implies that $c_s=\pm\iota a$ is pure imaginary. The long-wavelength "sound" excitations in (4.1) are no longer propagating. They combine into one unstable mode and one strongly damped mode with amplitudes behaving like $\exp[akt]$ and $\exp[-akt]$, respectively. This is the typical eigenvalue spectrum of the unstable modes in the Cahn-Hilliard theory [20] of spinodal decomposition. In Ref. [21] the eigenvalue spectrum of (5.1) has been solved numerically for all **k** values in the first Brillouin zone.

Outside the spinodal region the solution of the first-order eigenvalue problem gives for sound ($\mu=\sigma=\pm$) and shear modes ($\mu=\nu$)

$$z_\sigma^{(1)}=-\sigma c_s,\quad z_\nu^{(1)}=0 . \tag{5.8}$$

The corresponding right and left eigenvectors are

$$\begin{aligned} &|\psi_\sigma^{(0)}\rangle=|c_0^2+\sigma c_s c_l\rangle,\quad |\psi_\perp^{(0)}\rangle=|c_\perp\rangle ,\\ &\langle\tilde\psi_\sigma^{(0)}|=\langle c_s+\sigma c_l|,\quad \langle\tilde\psi_\perp^{(0)}|=\langle c_\perp| , \end{aligned} \tag{5.9}$$

where c_l and $c_\perp$ are seven-vectors with components c_{li} and $c_{\perp i}$ $(i=0,1,2,\ldots,6)$ and c_0 and c_s are constants, defined in (3.8). The nontrivial biorthogonality relations are

$$\begin{aligned} &\langle\tilde\psi_\sigma^{(0)}|\psi_{\sigma'}^{(0)}\rangle=6c_s\delta_{\sigma\sigma'} ,\\ &\langle\tilde\psi_\perp^{(0)}|\psi_\perp^{(0)}\rangle=3 . \end{aligned} \tag{5.10}$$

If the eigenvalue $z_\mu^{(1)}$ in (5.8) is inserted in (5.3), the equation is soluble and has the formal solution $|\psi_\mu^{(1)}\rangle=\Omega^{-1}|K^{(1)}\rangle$, where $|K^{(1)}\rangle$ is the inhomogeneous term in the first-order equation of (5.3), and Ω^{-1} the inverse of the collision operator in the orthogonal complement of the null space.

In absence of attractive interactions, obtained by setting $r=0$ in (5.7), one finds $c_s=c_0$. The right and left sound mode in (5.9) are the same apart from an overall normalization constant, and the eigenvectors $|\psi_\mu^{(0)}\rangle$ form an orthogonal set.

The scheme for solving the second-order equation (5.3) is the same as for the first order. The eigenvalue $z_\mu^{(2)}$ can be determined from the solubility condition $\langle a_n|K^{(2)}\rangle=0$, where $|K^{(2)}\rangle$ is the inhomogeneous term in the second-order equation. In fact, by using $\langle\tilde\psi_\mu^{(0)}|K^{(2)}\rangle=0$, one obtains a single equation for the damping coefficient,

$$z_\mu^{(2)}\langle\tilde{\psi}_\mu^{(0)}|\psi_n^{(0)}\rangle=-\langle\tilde{\psi}_\mu^{(0)}|\tfrac{1}{2}(c_l+z_\mu^{(1)})^2-\Lambda^{(2)}|\psi_\mu^{(0)}\rangle-\langle\tilde{\psi}_\mu^{(0)}|[c_l+z_\mu^{(1)}-\Lambda^{(1)}]\frac{1}{\Omega}[c_l+z_\mu^{(1)}-(1+\Omega)\Lambda^{(1)}]|\psi_\mu^{(0)}\rangle\ . \quad (5.11)$$

In deriving this result from (5.3) we have replaced $|\psi_\mu^{(1)}\rangle$ by the formal solution $\Omega^{-1}|\psi_\mu^{(0)}\rangle$ of the first-order equation in (5.3). We note in passing that $1/\Omega$ is the inverse of the Ω matrix in the orthogonal complement of its kernel.

B. Transport coefficients

Without the nonlocal attraction terms ($\Lambda^{(1)}=\Lambda^{(2)}=0$) Eq. (5.11) gives the standard expressions [16] for the kinematic viscosity, $z_\perp^{(2)}=\nu_0$, and the sound damping constant $z_\sigma^{(2)}=\gamma_0$ of the FHP III model, as will be shown first. In fact we find from (5.8) and (5.11) the damping coefficient of the shear mode,

$$z_\perp^{(2)}=\nu_0=-\left\langle c_l c_\perp\left|\frac{1}{\Omega}+\frac{1}{2}\right|c_l c_\perp\right\rangle\Big/\langle c_\perp|c_\perp\rangle$$
$$=\frac{1}{4}\left[\frac{1}{\omega_\nu}-\frac{1}{2}\right]. \quad (5.12)$$

In this and subsequent equations we use eigenvectors and eigenvalues of the FHP III collision operator [19]

$$\begin{aligned}&\Omega|c_l c_\perp\rangle=-\omega_\nu|c_l c_\perp\rangle\ ,\\ &\Omega|c_l^2-c_\perp^2\rangle=-\omega_\nu|c_l^2-c_\perp^2\rangle\ ,\\ &\Omega|\tfrac{1}{2}c^2-c_0^2\rangle=-\omega_\xi|\tfrac{1}{2}c^2-c_0^2\rangle\ ,\end{aligned} \quad (5.13)$$

where the eigenvalues ω_n are positive and

$$\begin{aligned}&\omega_\nu=\kappa_2(7-8\kappa_2)\ ,\\ &\omega_\xi=7\kappa_2(1-2\kappa_2)\ ,\end{aligned} \quad (5.14)$$

with $\kappa_2=f(1-f)$. In a similar manner the sound damping constant can be calculated from (5.11), (5.9), and (5.8) with the result

$$z_\sigma^{(2)}=\gamma_0=-\frac{1}{2}\left\langle c_l^2-c_0^2\left|\frac{1}{\Omega}+\frac{1}{2}\right|c_l^2-c_0^2\right\rangle\Big/\langle c_l|c_l\rangle\ , \quad (5.15)$$

where also the relations $c_s=c_0$ and $(c_l+z_\sigma^{(1)})\psi_\sigma^{(0)}=\sigma(c_l^2-c_0^2)$ have been used. The vector $c_l^2-c_0^2$ can be decomposed into the second and third eigenvectors in (5.13). The sound damping becomes then $\gamma_0=\frac{1}{2}(\nu_0+\zeta_0)$, where the bulk viscosity ζ_0 is

$$\zeta_0=-\left\langle\frac{1}{2}c^2-c_0^2\left|\frac{1}{\Omega}+\frac{1}{2}\right|\frac{1}{2}c^2-c_0^2\right\rangle\Big/\langle c_l|c_l\rangle$$
$$=\frac{1}{14}\left[\frac{1}{\omega_\xi}-\frac{1}{2}\right]. \quad (5.16)$$

To calculate the transport coefficients for the attractive LGA, the matrices $\Lambda^{(1)}$ and $\Lambda^{(2)}$ have to be taken into account in (5.11). This can be done using the properties (4.10) and (4.11) of Sec. IV B. The algebra is again lengthy, but straightforward, and we obtain for the *kinematic viscosity*

$$\nu=\frac{1}{4\omega_\nu}(1-\tfrac{1}{3}r\kappa_3)[1-r\kappa_3(1-\omega_\nu)]-\tfrac{1}{8}(1-r^2\kappa_2)$$
$$=\nu_0(1-\tfrac{1}{3}r\kappa_3)(1-r\kappa_3)+\tfrac{1}{12}r\kappa_3(1-\tfrac{1}{2}r\kappa_3)+\tfrac{1}{8}r^2\kappa_2\ . \quad (5.17)$$

For the sound damping constant we find $\gamma=\frac{1}{2}(\nu+\zeta)$ with a *bulk viscosity* of

$$\zeta=\zeta_0(1-\tfrac{4}{3}r\kappa_3)-\tfrac{1}{21}r\kappa_3+\tfrac{1}{4}r^2\kappa_2\ . \quad (5.18)$$

These results apply to the attractive LGA. For the repulsive model we use the duality transformation $f\leftrightarrow 1-f$ of Sec. II C, which implies in (5.17) and (5.18) that $\kappa_2\rightarrow\kappa_2$ and $\kappa_3\rightarrow-\kappa_3$. The transport coefficients are positive for all values of the density and the interaction range, and larger than the corresponding values at $r=0$. This can be seen by comparing Figs. 5 and 9 with Figs. 6 and 10, respectively.

Some remarks about the validity of the k expansion (5.2) are in order here. In the absence of long-range forces the k expansion of the kinetic equation is only meaningful when the streaming term is small compared to the collision term, i.e., $\|ik\cdot c\|\ll\|\Omega\|$. For small densities, $f=\rho/7$, the matrix elements of Ω are proportional to f, which imposes the constraint $k\ll f$ or $kl_0\ll 1$ where $l_0\sim 1/f$ is the mean free path.

The Taylor expansion (5.2) or (4.7) of the nonlocal interaction operator $\Lambda(k)$ imposes the second condition $kr\ll 1$. Hence the propagation speed and damping constants derived here only apply to long-wavelength disturbances with a wavelength large compared to mean free path l_0 and the force range r. The exact spectrum of (5.1) for arbitrary wave number $\mathbf{k}$ inside the first Brillouin zone and for arbitrary force range r will be discussed elsewhere [21].

VI. PRESSURE SIMULATIONS

A. Measurements

The equilibrium pressure can be measured by determining the trace of the microscopic momentum flux or stress tensor, $\tau_{\alpha\beta}(x)$, and averaging it over the equilibrium state, i.e.,

$$p=\frac{1}{2V}\sum_x\langle\tau_{\alpha\alpha}(x)\rangle\ , \quad (6.1)$$

where x runs over the whole lattice and V is the number of lattice sites. Additional space averaging, and eventually also time averaging, will further reduce the statistical noise. In our model $\mathbf{c}_i$ momentum is only transported in a direction parallel to $\mathbf{c}_i$. Let the microscopic momen-

tum flux be

$$\sum_x \tau_{\alpha\beta}(x) = \sum_{i=1}^{6} c_{i\alpha} c_{i\beta} (n_i + l_i) \ . \tag{6.2}$$

The first term, involving n_i, is the total momentum flux due to streaming; the second one, involving l_i, is the total flux due to the long-range interaction. The pressure is then

$$p = \frac{1}{2V} \sum_{i=1}^{6} \langle n_i + l_i \rangle \tag{6.3}$$

because $\mathbf{c}_i^2 = 1$. We determine the quantities n_i and l_i by counting the momentum flux at each time step. The quantity $\sum_{i=1}^{6} n_i$ is the number of particles having a nonzero velocity. This term enters because in one time step each one of these particles propagates over one lattice distance, transporting one unit of momentum.

The interactions (a) and (b) in Fig. 1 transfer one unit of $\mathbf{c}_j$ momentum over a distance r in the direction $-\mathbf{c}_j$, and the interaction (c) of Fig. 1 transfers two units. We determined $\sum_{i=0}^{6} l_i$ by counting the number of interactions of types (a) and (b) and multiplying the result with $-r$ and those of type (c) by $-2r$. For repulsive interactions the transport due to collisional transfer is in the opposite direction, and $-r$ should be replaced by $+r$.

To prepare the initial state we fill all velocity channels at random with a certain density and let the LGA fluid relax to equilibrium for a certain number of time steps. Then the pressure is measured over a period of 250 time steps, using the method described above. The results are averaged over 5 runs, and the error is estimated by the standard deviation, divided by $\sqrt{5-1}$.

B. Results

Figure 3 shows the results of our simulation with an attractive interaction having a range of 8 lattice sites, where $r_c \simeq 7.8$ is the critical value of the range r according to our mean-field theory, as shown in Sec. III B. For larger r values the mean-field equation for the pressure shows a van der Waals loop. Our results are represented by the triangles; the solid line is the theoretical prediction. Theoretically $dp/d\rho$ is negative between the densities $\rho = 1.22$ and $\rho = 1.75$, so the fluid has to separate into two phases. However, the effect is too small to show up in our measurements at a range of 8 lattice sites.

To get more significant results, which show the effect of phase separation, we did measurements for a fluid with an interaction range of 12 lattice sites. The results are shown in Fig. 2(a). The black triangles are the results of the simulations in which we started with a randomly filled lattice and let it relax for 3000 time steps.

The negative pressures at certain densities are a drawback of our model, but they are as predicted by the theory. In the spinodal range where $dp/d\rho < 0$, the results seem to lie on the horizontal line predicted by the Maxwell construction and not on the van der Waals curve. At these densities phase separation was observed. We note that for $dp/d\rho$ positive, the results lie on the van der Waals type curve instead of on the horizontal line, as one would expect from the Maxwell construction. At these densities the system seems to be in a metastable state. We also observe that the gas in the metastable region can be forced to phase separate by artificially making some local bubbles of the heavy or light phase.

For the densities 1.0 and 2.5 we also measured the pressure as function of time to see how the system evolves to equilibrium. In both cases we started with a randomly filled lattice. The results at $\rho = 2.5$ are shown in Fig. 4. For each point we averaged the pressure over 50 time steps and 5 runs. The horizontal line is the prediction of the Maxwell construction.

At the low density side, $\rho = 1.0$, the pressure exhibits strong fluctuations between 0.085 and $p_0 = 0.068$, which is the pressure at coexistence. The large fluctuations are typical of coexisting phases. Over a time interval of 2000 time steps we did not observe any approach to the pressure p_0. At density 2.5 about 700 time steps are needed to reach equilibrium.

We also observed the actual separation of the LGA fluid into bubbles of light and heavy phase, in agreement with the earlier observations of [2,3].

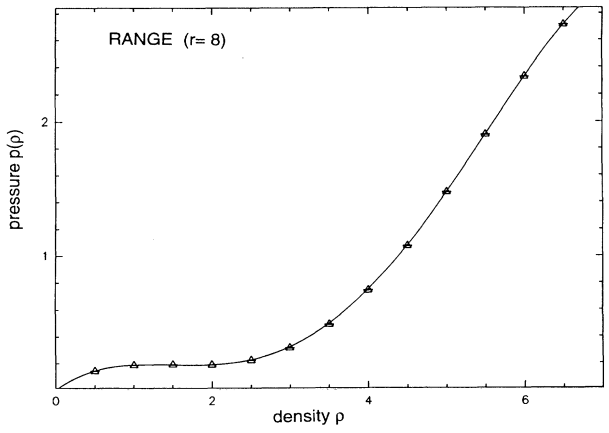

FIG. 3. Equation of state $p(\rho)$ at range $r = 8$, just above the critical range $r_c \simeq 7.8$, compared with computer simulations.

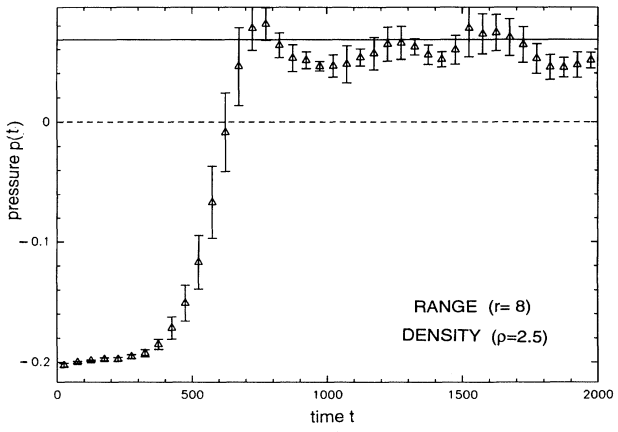

FIG. 4. Approach of simulated pressure to its value $p_0 \simeq 0.068$ at coexistence after initial preparation at uniform density $\rho = 2.5$.

VII. SIMULATIONS OF TRANSPORT COEFFICIENTS

A. Kinematic viscosity

To linear level the transverse velocity field relaxes as $g_\perp(k,t)=g_\perp(k,0)\exp[-\nu k^2 t]$, where $g_\perp(k,t)=\hat{\mathbf{k}}_\perp\cdot\mathbf{g}(k,t)$, is the transverse component of the momentum density, defined in (3.2). We use this relation to determine the shear viscosity, following the method used in [14].

At the initial time we set up a shear wave with a fixed wave vector $\mathbf{k}$. We then let the system relax by applying the dynamics. At regular time intervals we perform a Fourier transformation on the transverse velocity field. From the Fourier coefficients we determine the kinematic viscosity.

We shall now discuss this method in more detail. The macroscopic cell of our lattice gas is diamond shaped, L lattice units wide in the directions $\mathbf{c}_1$ and $\mathbf{c}_2$, where $L=256$ in our simulations. We apply periodic boundary conditions. The x axis is parallel to the basis vector $\mathbf{c}_1$ of the direct lattice; the y axis is parallel to a basis vector of the reciprocal lattice. We set up a shear wave in the y direction with wavelength, $\lambda=\frac{1}{2}L\sqrt{3}$. So we have a wave vector, $\mathbf{k}=2\pi\hat{\mathbf{y}}/[\frac{1}{2}\sqrt{3}\times 256]$, where $\hat{\mathbf{y}}$ is a unit vector in the positive y direction.

Preparation of the initial shear wave was done as follows: Let the origin of the Cartesian-coordinate system be in the lower left corner of the diamond, and let f be the reduced density of the LGA fluid. Then the rest particle states with $\mathbf{c}_0=\mathbf{0}$ are being filled with probability f. The states $\mathbf{c}_1$, $\mathbf{c}_2$, and $\mathbf{c}_6$ are filled with probability $f+a\sin(2\pi y/\lambda)$, where y is the y coordinate of the lattice site. The states $\mathbf{c}_3$, $\mathbf{c}_4$, and $\mathbf{c}_5$ are filled with probability $f-a\sin(2\pi y/\lambda)$. The density in the whole lattice is a constant, $\rho=7f$, but we have created a shear wave $g_\perp(\mathbf{k},0)=4a\sin(2\pi y/\lambda)$. We have chosen a sufficiently small so that no significant nonlinear effects could be observed in the dynamics.

Since we are only interested in waves with the previously described wave vector $\mathbf{k}$, the Fourier transformation of the transverse velocity field is performed at regular time intervals and is given by

$$g_\perp(k,t)=\sum_{x,y}\left[e^{-\iota y 2\pi/\lambda}\sum_{i=0}^{6}c_{ix}n_i(x,y,t)\right], \tag{7.1}$$

where $\lambda=\frac{1}{2}\sqrt{3}\times 256$. We perform a linear regression of the logarithm of these Fourier components versus the time. The slope gives us νk^2.

Figure 5 shows the results for the kinematic viscosity *without* a long-range interaction. We did five measurements with a length of 4000 time steps and a Fourier transformation after every 40 time steps to determine the viscosity at each density shown. The amplitude of the initial wave was $\frac{2}{7}$. The errors lie within the triangles. The dashed line is the theoretical prediction from the Boltzmann approximation.

The measured values of the kinematic viscosity (triangles) agree well with the simulation results of Ref. [16], which were also obtained by setting up a macroscopic initial shear wave. The FHP III model is self-dual, so that

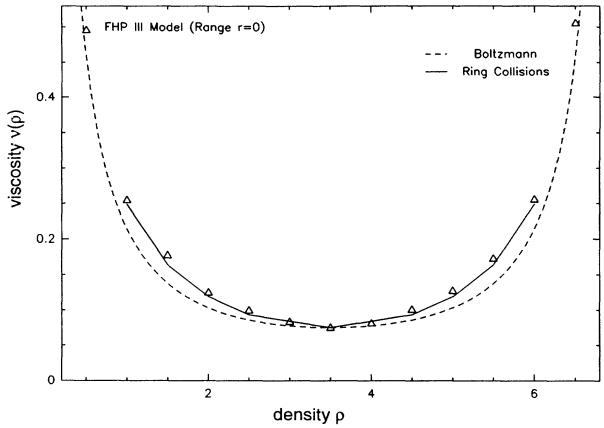

FIG. 5. Kinematic viscosity $\nu(\rho)$ for the FHP III model (only local interactions). Theoretical values from Boltzmann and ring kinetic theory are compared with computer simulations.

the graph is symmetric around $\rho=3.5$. The results are compared with the predictions from the Boltzmann equation (5.12), shown as dashed lines, and with those from the ring kinetic theory, evaluated by van Velzen, Brito, and Ernst [22]. The transport coefficients ν and γ were calculated at the same densities where the simulations have been performed. To guide the eye the points representing the results from ring kinetic theory are connected by straight line segments. The Boltzmann equation neglects all correlations between colliding particles, i.e., the molecular chaos assumption is made at every time step. The ring equation of Ref. [22] represents the simplest sequences of correlated collisions. It accounts for approximately 60% of the observed deviations between simulations and Boltzmann approximation.

The results of the simulations with long-range interactions are given in Figs. 6 and 7. All errors are within the symbols. The lines are the predictions of the viscosity in the Boltzmann approximation, as calculated in Sec. V B. In Fig. 6 we show the results as a function of the density

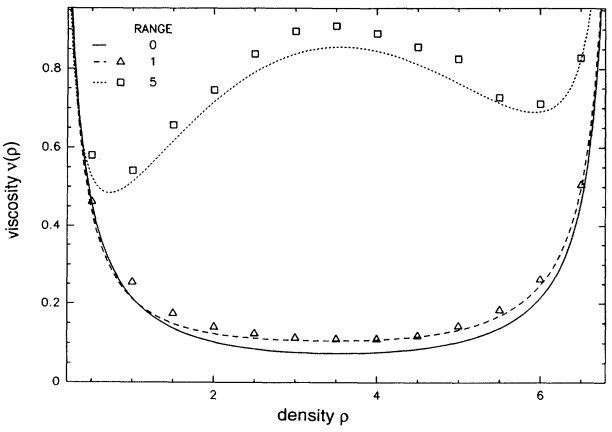

FIG. 6. Kinematic viscosity $\nu(\rho)$ in model with nonlocal attraction of range $r=0$, 1, 5. Boltzmann results are compared with computer simulations.

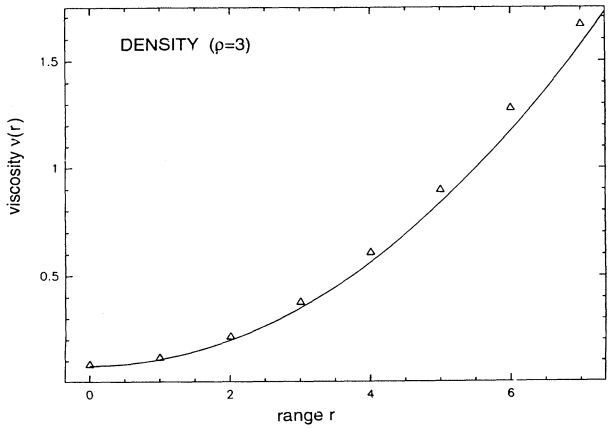

FIG. 7. Boltzmann value of kinematic viscosity $\nu(\rho)$ as a function of the range r at density $\rho=3$, compared with simulation results.

ρ for different ranges of the attractive force ($r=0,1,5$). The solid line corresponds to range $r=0$ (the same data are shown in Fig. 5 as a dashed line together with the simulations for $r=0$). Within the present theory we cannot decide whether the deviations at larger r values (see Figs. 6 and 7 with $r=5$) are due to the breakdown of the assumption, $kr \ll 1$, or are a consequence of the mean-field assumption that neglects the correlations between colliding particles.

Figure 7 shows the viscosity as a function of the range r at a fixed density $\rho=3$. The agreement between the simulations and the mean-field theory for the LGA with attractive interactions is surprisingly good. In fact the quantitative predictions of the Boltzmann approximation for transport coefficients in local and nonlocal interaction models are of equal quality when compared with results of computer simulations.

B. Propagation and damping of sound

We use a similar method to determine the sound damping coefficient $\gamma=\frac{1}{2}(\nu+\zeta)$. Macroscopically the sound modes are Fourier components of the deviations from equilibrium in the number density $\delta\rho(k,t)$ and in the longitudinal momentum density $g_l(k,t)=\hat{\mathbf{k}}\cdot\mathbf{g}(k,t)$. They decay as

$$c_s\delta\rho(k,t)+\sigma g_l(k,t) = [c_s\delta\rho(k,0)+\sigma g_l(k,0)]e^{-(\iota\sigma c_s k+\gamma k^2)t} . \quad (7.2)$$

We start with a longitudinal velocity wave with the same wave vector as for the shear wave. The density is constant initially, so that $\delta\rho(k,0)=0$. The relaxation of the longitudinal velocity field and the density field are described by

$$g_l(k,t)=g_l(k,0)\cos(c_s kt)e^{-\gamma k^2 t} ,$$
$$\delta\rho(k,t)=(\iota/c_s)g_l(k,0)\sin(c_s kt)e^{-\gamma k^2 t} . \quad (7.3)$$

The initial longitudinal wave is prepared in the same manner as the shear wave. We chose the same wave vector $\mathbf{k}$. The states $\mathbf{c}_0$, $\mathbf{c}_1$, and $\mathbf{c}_4$ are filled with probability f. The probability for the states $\mathbf{c}_2$ and $\mathbf{c}_3$ is $f+a\sin(2\pi y/\lambda)$ and for the states $\mathbf{c}_5$ and $\mathbf{c}_6$ is $f-a\sin(2\pi y/\lambda)$. The initial density field is constant, so that we have a longitudinal wave with amplitude $g_l(k,0)=2a\sqrt{3}\sin(2\pi y/\lambda)$.

At each time step we perform a Fourier transformation of the longitudinal velocity field and density field for the wave vector $\mathbf{k}$:

$$g_l(k,t)=\sum_{x,y}\left[e^{-\iota y 2\pi/\lambda}\sum_{i=0}^{6}c_{iy}n_i(x,y,t)\right] ,$$
$$\delta\rho(k,t)=\sum_{x,y}\left[e^{-\iota y 2\pi/\lambda}\sum_{i=0}^{6}[n_i(x,y,t)-\rho_0]\right] . \quad (7.4)$$

We deduce the velocity of sound from the time between the zero crossings of $g_l(k,t)$ and $\delta\rho(k,t)$. The velocity of sound is given by $c_s=\lambda/2T$, where T is the time between two successive zeros and $\lambda=\frac{1}{2}\sqrt{3}\times 256$ is the wavelength.

At times mT, where T is again the time between two successive zeros and m an integer, the absolute value of the longitudinal wave behaves like $|g_l(k,mT)| = C_1\exp[-\gamma k^2 mT]$. At times $\frac{1}{2}T+mT$ the density wave behaves like $|\delta\rho(k,\frac{1}{2}T+mT)|=C_2\exp[-\gamma k^2(\frac{1}{2}T+mT)]$ with C_1 and C_2 constants. So in a similar manner as in Sec. VII A we can deduce γ from the longitudinal velocity wave and the density wave at the specified times.

We perform a linear regression of the logarithm of the absolute value of the Fourier components $g_l(k,t)$ at times $t=MT$, and γk^2 can be determined from the slope. We do the same for $\delta\rho(k,t)$ at times $t=\frac{1}{2}T+mT$. Our final result is the mean of these two values for γ.

Figure 8 shows the results for the velocity of sound for different interaction ranges in the attractive model, where the system does not phase separate. We did five runs with a length of 3000 time steps to determine each point.

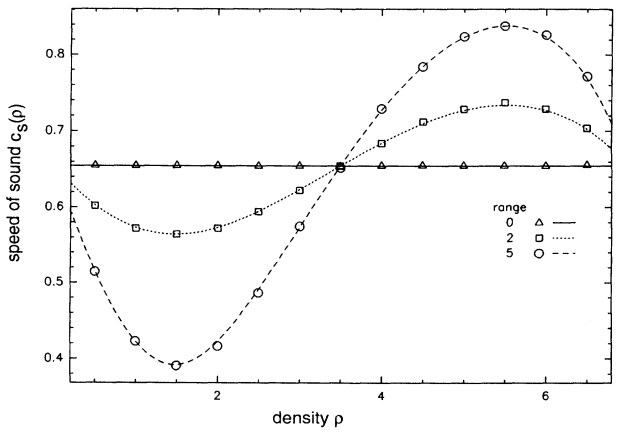

FIG. 8. Speed of sound $c_s(\rho)$ is the attractive model at range $r=0,2,5$.

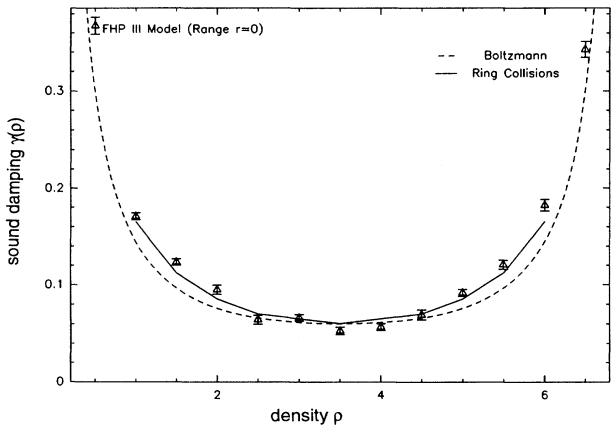

FIG. 9. Sound damping constant $\gamma(\rho)$ for the FHP III model (only local interactions). Theoretical values from Boltzmann and ring kinetic theory are compared with computer simulations.

The amplitude of the longitudinal velocity wave is $\sqrt{3}/28$. These results are in perfect agreement with the theoretical predictions of the mean-field theory.

In Fig. 9 we show the simulation results for the sound damping constant $\gamma=\frac{1}{2}(\nu+\zeta)$ in the standard FHP III model with range $r=0$. They are in general agreement with the measurements in Ref. [16]. The data are extracted from the same data as the speed of sound. The results are compared with the Boltzmann approximation (dashed lines) and with the simple ring approximation of Ref. [22]. The simple ring approximation accounts again for about 60% of the observed deviations between simulations and Boltzmann approximation.

In Fig. 10 we show the results for the sound damping coefficient for the model with finite-range attraction and a comparison with the predictions from mean-field theory. Results are shown for a range of 2 and 5 lattice sites. The statistical errors are bigger for longer ranges. Also the errors are large in comparison with the results for the shear viscosity. This is probably due to our method of

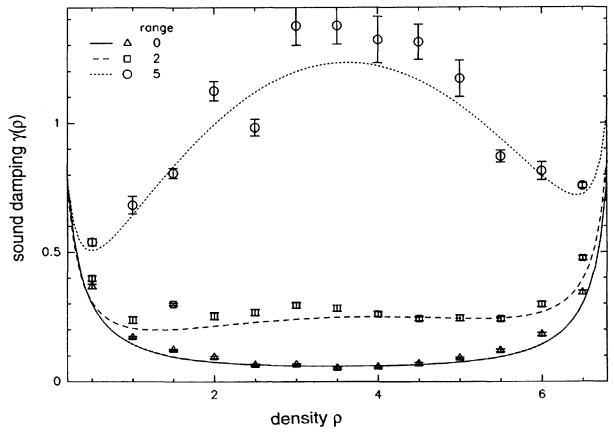

FIG. 10. Sound damping constant $\gamma(\rho)$ in the model with nonlocal attraction of range $r=0$, 1, 5. Boltzmann results are compared with computer simulations.

extracting the sound damping coefficient from the data. We used fewer points to determine this coefficient than we did to determine the kinematic viscosity. For smaller values for the velocity of sound, we have fewer points to determine the sound damping coefficient. For short ranges (see Fig. 10 with $r=2$) the predictions of the Boltzmann equation are quite good. For larger ranges (see Fig. 10 with $r=5$) the deviations start to grow.

VIII. CONCLUSIONS AND PROBLEMS

In this paper we have modeled finite-range attractive or repulsive interactions in the context of lattice-gas automata by modifying the standard triangular FHP III model and we have studied its equilibrium and transport properties. The model does not conserve energy. It has no temperature, and internal or free energy are not thermodynamic state functions. The model does not obey the detailed balance conditions. This can be seen as follows. Take for instance the (a) collision of Fig. 1. The left configuration A goes with probability 1 into the right configuration B. The right configuration B on the other hand goes with probability 1 into itself. The transition from B to A is impossible. Therefore the total probability (summed over all input states) to find configuration A as an output state in the long-range interaction step is smaller than unity. Consequently, the semidetailed balance condition [1] is also violated.

For this model a theoretical description is given of transport through collisional transfer in LGA's, i.e., instantaneous transfer of momentum over the range r of the interaction. If the range of interaction—it may be attractive or repulsive—is sufficiently large, the equation of state for the pressure has a loop of the van der Waals type. There are metastable and unstable branches. We apply the Maxwell construction to obtain the stable equilibrium states of coexisting high and low density phases. The measured values of the pressure are in good agreement with the equation of state for this model, even in the two-phase region. We also observed the actual phase separation in bubbles of high and low density.

However, there is a conceptual problem here, because there is no justification for applying the Maxwell construction to the kinetic pressure. The Maxwell construction is based on the thermodynamic pressure being a derivative of some thermodynamic potential (e.g., free energy) that has an extremum for a stable equilibrium state. Furthermore the partition function and thermodynamic potential cannot be calculated, because the equilibrium state is unknown for models that violate detailed or semidetailed balance.

The model with nonlocal repulsion is simply the dual of the one with attraction. Its macroscopic properties are related by the duality transformation, $f\rightleftarrows 1-f$. If the model with attraction has a phase transition, the one with repulsion has a phase transition as well. This is illustrated in Figs. 2(a) and 2(b).

The analysis of the nonequilibrium properties of the model is based on the nonlinear Boltzmann equation, in which the molecular chaos assumption is made in the local and in the finite-range collision terms. For the first time analytical results have been obtained for the trans-

port coefficients in such models. This has been done by linearizing the Boltzmann equation around the uniform equilibrium state and determining the eigenmodes. The eigenvalues for small k yield the speed of sound, sound damping constant γ, and kinematic viscosity ν. The transport coefficients contain contributions linear and quadratic in the range r of the nonlocal interaction operator Λ. Very recently similar results have been obtained by Appert, Zaleski, and d'Humières [15].

Apart from the equation of state we have also measured transport coefficients. The viscosity and sound damping constant were obtained from the damping of a sinusoidal disturbance in the transverse and in the longitudinal flow field, respectively. In the single-phase region the measured speed of sound is in excellent agreement with both the pressure measurements as well as with the theoretical predictions. Also the measured transport coefficients agree well with the theoretical predictions for short ranges of the nonlocal interactions. For longer ranges there are effects of generalized hydrodynamics with wave-number-dependent transport coefficients.

The agreement of theory and simulations is remarkable for the long-range interaction models although they lack semidetailed balance. In fact microstates are lost in the nonlocal interaction step. The fundamental question is now: Do the local collision step and the propagaqtion step replenish the microstates, lost in the nonlocal interaction step, or is the final equilibrium state living in a contracted space of much lower dimensionality, as seems to be the case in the biased LGA of Ref. [23]? The equilibrium state of such a model is not known. Here we treated the problem only in mean-field approximation, in which the correlation between fluctuations is totally neglected.

ACKNOWLEDGMENTS

The work of FOM Institute is part of the scientific program of the "Stichting voor Fundamenteel Onderzoek der Materie (FOM)," which is financially sponsored by the "Nederlandse Organisatie voor Wetenschappelijk Onderzoek (NWO)."

[1] U. Frisch, D. d'Humières, B. Hasslacher, P. Lallemand, Y. Pomeau, and J. P. Rivet, Complex Systems **1**, 649 (1987) [reprinted in *Lattice Gas Methods for Partial Differential Equations,* edited by G. Doolen (Addison-Wesley, Singapore, 1990), p. 77].
[2] C. Appert and S. Zaleski, Phys. Rev. Lett. **64**, 1 (1990).
[3] C. Appert and S. Zaleski (unpublished).
[4] H. Chen, S. Chen, G. D. Doolen, Y. C. Lee, and H. A. Rose, Phys. Rev. A **40**, 2850 (1989).
[5] M. H. Ernst, in *Fundamental Problems in Statistical Mechanics VII,* edited by H. van Beijeren (Elsevier Science Publishers B. V., Amsterdam, 1990), p. 321.
[6] M. H. Ernst and S. P. Das, J. Stat. Phys. **66**, 465 (1992).
[7] C. Cercignani (unpublished).
[8] R. Brito, M. H. Ernst, and T. R. Kirkpatrick, in *Discrete Models of Fluid Dynamics,* edited by A. S. Alves, Series on Advances in Mathematics for Applied Sciences (World Scientific, Singapore, 1991), p. 198; M. H. Ernst, in *ibid.*, p. 186.
[9] E. C. G. Stueckelberg, Helv. Phys. Acta **25**, 577 (1952).
[10] W. Heitler, Ann. Inst. Henri Poincaré **15**, 67 (1956).
[11] D. Rothman and S. Zaleski, J. Phys. (Paris) **50**, 2161 (1989).
[12] F. J. Alexander, I. Edrei, P. L. Garrido, and J. L. Lebowitz, J. Stat. Phys. **68**, 497 (1992).
[13] H. J. Bussemaker and M. H. Ernst, J. Stat. Phys. **68**, 431 (1992).
[14] B. Dubrulle, U. Frisch, M. Hénon, and J. P. Rivet, J. Stat. Phys. **59**, 1187 (1990).
[15] C. Appert, S. Zaleski, and D. d'Humières (unpublished).
[16] D. d'Humières and P. Lallemand, Complex Systems **1**, 633 (1987) [see also *Lattice Gas Methods for Partial Differential Equations,* Ref. [1], p. 299].
[17] S. Chapman and T. G. Cowling, *The Mathematical Theory of Nonuniform Gases* (Cambridge Univ. Press, Cambridge, 1970).
[18] P. Resibois and M. de Leener, *Classical Kinetic Theory of Fluids* (Wiley, New York, 1977).
[19] R. Brito, M. H. Ernst, and T. R. Kirkpatrick, J. Stat. Phys. **62**, 283 (1991).
[20] K. Binder, in *Phase Transformation in Materials,* edited by P. Haasen, Material Science and Technology (VCH Verlagsgesellschaft, Weinheim, Germany), Vol. 5, Chap. 7.
[21] H. J. Bussemaker and M. H. Ernst (unpublished).
[22] G. A. van Velzen, R. Brito, and M. H. Ernst, J. Stat. Phys. **70**, 811 (1993).
[23] H. J. Bussemaker and M. H. Ernst, Physica A **194**, 258 (1993).